minerals

MDPI

Article

Effect of Ca^{2+} Replacement with Cu^{2+} Ions in Brushite on the Phase Composition and Crystal Structure

Mazen Alshaaer [1], Juma'a Al-Kafawein [2], Ahmed S. Afify [3], Nagat Hamad [1], Ghassan Saffarini [4] and Khalil Issa [5,*]

[1] Department of Physics, College of Science and Humanities in Al-Kharj, Prince Sattam bin Abdulaziz University, Al-Kharj 11942, Saudi Arabia; m.alshaaer@psau.edu.sa (M.A.); n.hamad@psau.edu.sa (N.H.)
[2] Department of Chemistry, King Faisal University, Al-Hassa 31982, Saudi Arabia; jalkafawein@kfu.edu.sa
[3] Department of Basic Sciences, Higher Institute of Engineering and Automotive and Energy, Technology, New Heliopolis 11829, Egypt; ahmed.afify@polito.it
[4] Department of Physics, An-Najah National University, Nablus 00972, Palestine; safarini@najah.edu
[5] Orthopedics Unit, Faculty of Medicine and Health Sciences, An-Najah National University, Nablus 00972, Palestine
* Correspondence: k.issa@najah.edu; Tel.: +970-5992-08667

Abstract: The gradual replacement of Ca^{2+} with Cu^{2+} ions in brushite ($CaHPO_4{\cdot}2H_2O$) has been extensively studied and discussed. The approach adopted in this work has not been systematically explored in previous studies. This novel approach may prove beneficial for the production of $Ca_{1-x}Cu_xHPO_4{\cdot}nH_2O$ materials with desired properties suitable for medical applications. Solutions of sodium dihydrogen orthophosphate dihydrate, $NaH_2PO_4{\cdot}2H_2O$, calcium nitrate tetrahydrate, $Ca(NO_3)_2{\cdot}4H_2O$, copper nitrate trihydrate, $Cu(NO_3)_2{\cdot}3H_2O$, ammonium hydroxide solution, and diluted HCl were used for the preparation of these materials. At low Cu/Ca molar ratios (up to 0.25) in the starting solution, biphasic phosphate minerals were formed: brushite and sampleite. When the Cu/Ca molar ratio increases gradually from 0.67 to 1.5, sampleite-like mineral precipitates. Powdered XRD (X-ray diffraction), thermogravimetric (TG) analysis, and SEM (scanning electron microscopy) techniques were employed for the study of the microstructure of the produced materials for different degrees of Ca replacement with Mg. It is found that the Cu/Ca ratio in the starting solution can be adjusted to obtain materials with tailored composition. Thus, a new method of sampleite-like synthesis as a rare mineral is introduced in this study. Both phosphate minerals brushite and sampleite-like minerals are attractive as precursors of bioceramics and biocements. The search for such products that may decrease the possibility of post prosthetic or implant infection can be crucial in preventing devastating post-surgical complications.

Keywords: brushite; sampleite; biomaterials; XRD; crystal growth

Citation: Alshaaer, M.; Al-Kafawein, J.; Afify, A.S.; Hamad, N.; Saffarini, G.; Issa, K. Effect of Ca^{2+} Replacement with Cu^{2+} Ions in Brushite on the Phase Composition and Crystal Structure. *Minerals* **2021**, *11*, 1028. https://doi.org/10.3390/min11101028

Academic Editors: Oluwatoosin Agbaje and Olev Vinn

Received: 25 August 2021
Accepted: 17 September 2021
Published: 22 September 2021

1. Introduction

Calcium phosphate-based minerals (CaPs) are used in various environmental, medical, and engineering sciences applications. They may substitute bone in medical applications [1,2], because their mineralogical structure and biochemical properties are similar to the mineral phases present in bone tissues. Their low toxicity, high bioactivity, and excellent biocompatibility nominate them as precursors for the preparation of biocements and bioceramics, which exhibit high potential for applications in the fields of advanced materials and technology [3,4]. Thus, CaPs are excellent candidates for bone tissue engineering, drug delivery, and bone-related disease treatment [5,6]. Additionally, CaPs may be used as fertilizers [7] or construction materials [8,9].

One of the best-known CaPs is brushite (dicalcium phosphate dihydrate (DCPD, $CaHPO_4.2H_2O$) [8,10], which is stable in a weakly acidic environment (pH 4.0–6.5) and low temperature (less than 80 °C) [11,12]. It can be produced under a specific temperature

and pH range and is usually metastable at physiological conditions, pH ≈ 7.4, so that it can be resorbed within relatively short periods and form bone material [13,14]. In addition, brushite is an important precursor for the formulation of several bone cements and bioceramics [10–14].

Brushite-based materials and cements exhibit good bioactivity, and they are bioresorbable and biocompatible. Unlike apatite-based materials, brushite-based ones are rapidly resorbed in vivo [13]. Being an acidic mineral, brushite can only precipitate from solutions at low pH (less than 6.5); hence, the initial phase of its setting reactions is very rapid [14]. Therefore, inhibitors of crystal nucleation and growth such as hydroxyapatite and tricalcium phosphates are used to control the setting reactions. The bioactivity and biocompatibility of brushite-based materials has been investigated in several compositions, applications, compositions, and in vivo [10,11]. Brushite-based materials are biocompatible with and tolerated by soft tissues and bone in vivo, so that material resorption was shortly followed by the formation of new bone tissues. Histological measurements and experimental studies indicate that brushite-based materials feature good biocompatibility, with no appearance of inflammatory cells [13].

Late prosthetic joint infections (PJIs) pose an increasing medical challenge as more and more joint replacements are being performed, and patients' life expectancy increases [15]. Continuous efforts are needed to ameliorate such devastating complications. Currently, copper [16,17] is seriously considered in view of its antibacterial contact-killing effect and microbial properties; a most common point in the literature is that all copper-exposed bacteria have survival regimens of just a few minutes before cell death. No complete resistance to prolonged exposure with copper has been found [18–21].

Therapeutic metallic elements such as copper are direly needed and widely used in biomedicine [17], given the ease of their incorporation into different types of biomaterials. Specifically, great opportunities for biomedical engineers and clinicians are offered by copper-doped bioactive glasses because of their excellent regenerative potential and biocompatibility [22]. Accelerated soft tissue healing can be achieved with copper-incorporated bioactive glasses, showing noteworthy potential for wound treatment and skin repair, besides their known usefulness in bone tissue engineering. Copper has the ability to modify the physicochemical properties of bioactive glasses (e.g., reactivity with bio-fluids) and thus enhance their potential therapeutic uses. Copper-doped bioactive glasses may reduce or even prohibit bacterial growth, improve cell proliferation, and promote angiogenesis. Their suitability in cancer photothermal therapy (PTT) has been described recently [21]. Yet to obtain knowledge regarding the extent to which copper-doped bioactive glasses are actually applicable for tissue engineering and regenerative medicine strategies in the clinical setting, further research is needed. Moreover, the use of copper-doped bioactive glasses in combination with polymers to produce relatively soft, pliable composites and printable inks for use in biofabrication [22,23] holds promise for the future. Accordingly, sampleite [24], a Cu-rich mineral, might be used as a precursor of bone cements and ceramics.

The replacement (exchange) of ions is known to occur in crystals when their radii and valences are similar [10]. Although Cu^{2+} has a smaller ionic radius than Ca2+ (1.3 and 1.8 Å, respectively), these two ions are able to replace each other in a crystal [23–25]. The substitution and doping of Ca^{2+} with Cu^{2+} in CaPs has been previously investigated [26]. A partial substitution of Ca^{2+} by Cu^{2+} in bioceramics and bone cements may enhance cell growth and proliferation as well as decrease bone resorption and contribute to sustainable bone formation [4,26–28].

In-depth analysis was carried out here to investigate the crystal morphology, chemical composition, and mineralogy of the phosphate minerals produced when different Cu/Ca molar ratios are used in the starting solution. As the motivation behind our research, such aspects will hopefully prove beneficial and contribute to the future synthesis of biomaterials with tailored properties.

2. Experimental Methodology

2.1. Materials

Calcium nitrate tetrahydrate and copper(II) nitrate trihydrate came from LOBA Chemie, India, while sodium dihydrogen orthophosphate dihydrate ($NaH_2PO_4 \cdot 2H_2O$) was purchased from Techno Pharmchem, India. A water purification system (PURELAB option-Q, ELGA, High Wycombe, UK) was used to prepare distilled water (0.055 μS/cm). Each component was weighed using a digital analytical balance (EX324N, OHAUS, Parsippany, NJ, USA). Stirring was performed with the use of a magnetic stirrer (ISOTEMP, Fisher Scientific, Shanghai, China).

2.2. Preparation of Calcium–Copper Phosphate Minerals

The preparation of phosphate minerals was carried out at ambient conditions, with the use of three solutions, namely $Cu(NO_3)_2 \cdot 3H_2O$, $Ca(NO_3)_2 \cdot 4H_2O$, and $Na_2HPO_4 \cdot 2H_2O$ 0.5 mol/L. The molar proportions used in each case for the synthesis of $Ca_xCu_{1-x}.HPO_4 \cdot nH_2O$ with different composition are shown in Table 1.

Table 1. Molar proportions of $Cu(NO_3)_2 \cdot 3H_2O$, $Ca(NO_3)_2 \cdot 4H_2O$, and $NaH_2PO_4 \cdot 2H_2O$ as well as Cu/Ca molar ratios used for the synthesis of calcium–copper phosphate compounds.

Product ID	$NaH_2PO_4 \cdot 2H_2O$	$Ca(NO_3)_2 \cdot 4H_2O$	$Cu(NO_3)_2 \cdot 3H_2O$	Cu/Ca Molar Ratio
BCu0	1	1	0	0
BCu2	1	0.8	0.2	0.25
BCu4	1	0.6	0.4	0.67
BCu5	1	0.5	0.5	1.0
BCu6	1	0.4	0.6	1.5
BCu10	1	0	1	-

First, pure brushite, BCu0, was produced by the dropwise addition of 100 mL $Ca(NO_3)_2 \cdot 4H_2O$ solution (flow rate ≈ 2 mL/min), using a glass funnel with a glass stopcock, to the $Na_2HPO_4 \cdot 2H_2O$ solution under continuous stirring (stirring speed 450 rpm) until a Ca/P molar ratio of 1.0 was obtained. To enable full homogeneity, the new solution was stirred at room temperature for 1 h. The total stirring period prior to filtering was about two hours. The pH of the solution was adjusted to values ranging between 6 and 6.5, see Figure 1, in order to enable the production of a white precipitate. Then, this precipitate was vacuum-filtered using a Buchner funnel and qualitative filter paper (45 μm, ∅ 12 cm, Double Rings, Shanghai, China). The filter cake was washed three times with de-ionized water and three more times with ethanol to prevent agglomeration [29,30]. Afterwards, it was placed on a watch glass and dried for 5 days in an oven (ED53/E2, Binder, Tuttlingen, Germany).

BCu2, BCu4, BCu5, and BCu6 compounds were prepared by mixing, first, the $Ca(NO_3)_2 \cdot 4H2O$ and $Cu(NO_3)_2 \cdot 3H_2O$ solutions using the molar ratios shown in Table 1. Then, 100 mL of the obtained solution was added dropwise to 100 mL of $Na_2HPO_4 \cdot 2H_2O$ solution, as previously described. Finally, BCu10 was obtained after mixing $NaH_2PO_4 \cdot 2H_2O$ and $Cu(NO_3)_2 \cdot 3H_2O$ by means of the same procedure.

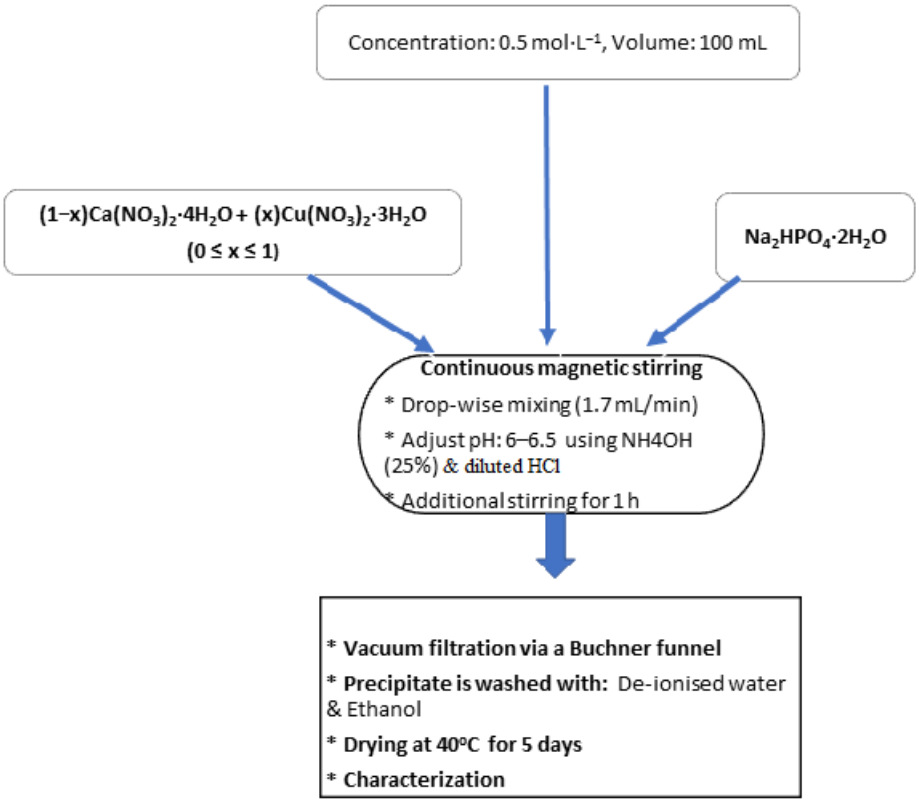

Figure 1. Preparation of calcium–copper phosphates.

2.3. Characterization Techniques

The phase composition of the products was carried out qualitatively using a Shimadzu XRD diffractometer−6000 (manufacturer, Nakagyo-ku, Kyoto, Japan) with a cobalt tube and a scanning 2-theta range from 100 to 600 at a scan rate of 2 °/min. The Match! Software package Version 2.4.7 (Crystal Impact, Bonn, Germany) was used for Rietveld refinement and phase analyses of powder X-ray diffraction (XRD) data. To identify product morphology, a scanning electron microscope (Inspect F50, the Netherlands) was used. A thermogravimetric (TG) analyzer (TG 209 F1 Libra, NETZSCH, Selb, Germany), during heating in the temperature range from 40 to 600 °C with a heating rate of 5 °C min^{-1} under a helium atmosphere, was used to determine the mass loss of each product (≈100 mg).

3. Results and Discussion

3.1. Mineralogical and Microstructural Analysis

Figure 2 depicts the XRD patterns of all the synthesized materials. The mineralogy of BCu0 confirms that this precipitate, produced after mixing $NaH_2PO_4{\cdot}2H_2O$ and $Ca(NO_3)_2{\cdot}4H_2O$ solutions with a Ca:P molar fraction 1:1 (Table 1), is pure brushite [31–34]. It is observed that the crystals of brushite grow in proportion to the major planes, namely (141), (121), and (020). The XRD pattern of the BCu0 denotes brushite's monoclinic structure [12,29]. The crystal growth takes place primarily along the (020) crystallographic plane [4] as evidenced from the peak at 2-theta 11.7° [35,36].

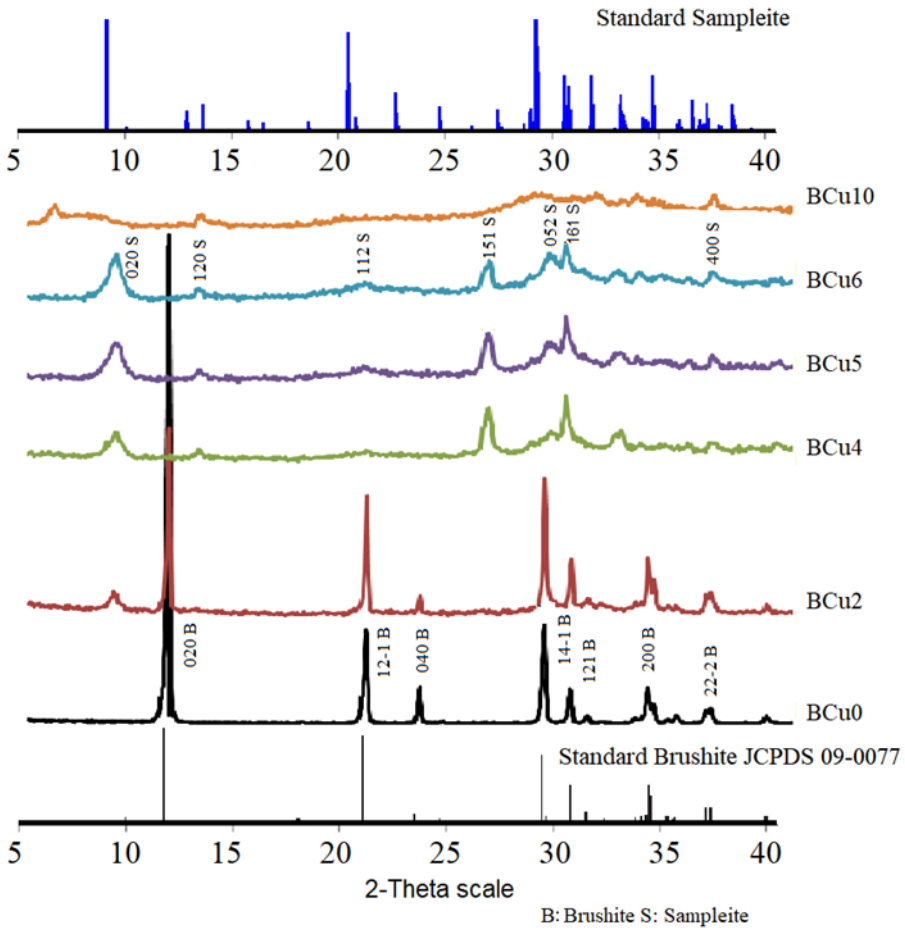

Figure 2. XRD patterns of the calcium–copper phosphates (Table 1).

The pattern of BCu2, obtained on the material prepared with low Cu/Ca molar ratio (0.25), indicates the presence of biphasic phosphate brushite ($CaHPO_4 \cdot 2H_2O$) and sampleite-like mineral ($NaCaCu_5(PO_4)_4Cl \cdot 5(H_2O)$). A new XRD peak corresponding to sampleite-like mineral appeared at plane (020). The brushite peaks present, and their intensity, especially for those associated with the plane (020), decreased.

The gradual increase from 0.25 to 1.0—and eventually to 1.5 (patterns BCu4 to BCu6)—in the Cu/Ca molar ratio in the starting solution led to an increase in the degree of Ca replacement with Cu. Simultaneously, brushite disappeared, and only sampleite-like mineral precipitated. Thus, at higher molar ratios, the intensity of sampleite-like mineral peaks would increase in the XRD patterns. Eventually, a semi-crystalline structure in the pattern of BCu10 of the precipitate formed when a Cu/P ratio of 1.0 was used.

Figure 3 shows photographs of the Ca-Cu phosphate compounds produced in this research. Typical for pure CaPs, brushite appears as a white powder; see Figure 3A, Bcu0 [30]. The second compound, Figure 3B, is white in color with a clear presence of blue tones, but in smaller quantities, indicating the presence of the two minerals together: brushite (white) and sampleite (blue) [33]; see Figure 3. In turn, the compounds BCu4–BCu6 turn blue with an increased amount of copper, as shown in Figure 3C–E, where only the sampleite–like mineral is present. Finally, the blue compound Bcu10 appears after complete replacement of calcium with copper; see Figure 3F.

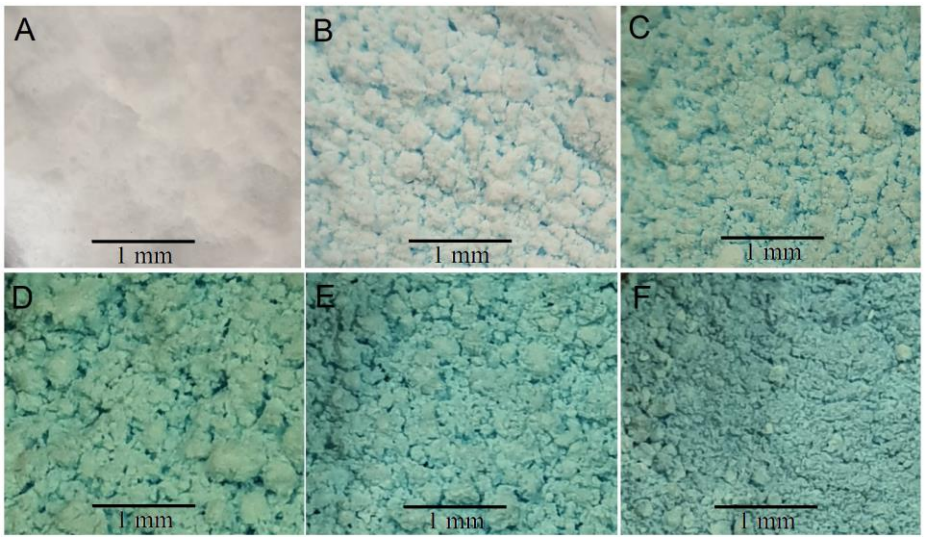

Figure 3. Images obtained by optical microscopy (Optika, Italy) of Ca-Cu phosphates, (**A**) BCu0, (**B**) BCu1, (**C**) BCu4, (**D**) BCu5, (**E**) BCu6, and (**F**) BCu10 (all images have the same 1 mm scale bar).

Rietveld-refined unit cell parameters for brushite- and sampleite-like materials are presented in Tables 2 and 3. It is seen that the unit cell parameters of brushite increase for the materials BCu0–BCu2 (Table 2), which were produced using the Cu/Ca molar ratio in the starting solution up to 0.25, and in which brushite was the dominant phase formed. In contrast, for the materials having a Cu/Ca molar ratio above 0.25, brushite disappeared completely, and a new sampleite-like mineral phase is formed. The unit cell parameters of sampleite exhibited an increasing Cu/Ca molar ratio, from 0.25 to 0.67; see Tables 2 and 3. The unit cell parameters of sampleite were constant, increasing the Cu/Ca molar ratio in the starting solution from 0.67 up to 1.5, where sampleite is the only crystalline mineral, BCu4–BCu6, Table 3.

Table 2. The parameters of unit cell for brushite from XRD data (Rietveld refinement).

Product ID	Brushite wt%	a(Å)	b(Å)	c(Å)	(β°)	V(Å^3)
BCu0	100.0	5.8145	15.1693	6.2399	116.392	523.88
BCu2	80.7	5.8132	15.1973	6.2497	116.406	527.87
BCu4	0.0	-	-	-	-	-
BCu5	0.0	-	-	-	-	-
BCu6	0.0	-	-	-	-	-
BCu10	0.0	-	-	-	-	-

Table 3. The parameters of unit cell for sampleite-like mineral from XRD data (Rietveld refinement).

Product ID	Sampleite wt%	a(Å)	b(Å)	c(Å)	(β°)	V(Å^3)
BCu0	0.0	-	-	-	-	-
BCu2	19.3	9.6950	19.7390	9.6730	102.610	80.74
BCu4	100.0	9.6760	19.2840	9.7660	90.070	127.45
BCu5	100.0	9.6760	19.2840	9.7660	90.070	127.45
BCu6	100.0	9.6760	19.2840	9.7660	90.070	127.45
BCu10	0.0	-	-	-	-	-

The quality of the Rietveld refinement was acceptable for all materials studied (RBrag < 8%, χ^2 < 2), but there is a lack of database material regarding sampleite mineral. In general, the reported findings resemble data obtained in earlier recent studies focusing on the production of brushite [28] or sampleite [34].

SEM images of the various Ca-Cu phosphates, obtained for different Cu/Ca molar ratios present in solution, are shown in Figure 4. The morphology of pure brushite (BCu0), biphasic brushite-samplete-like compound (BCu2), sampleite-like (BCu4, BCu5, and BCu6), and semi-crystalline structured (BCu10) are shown in Figure 4A–F. The precipitation of plate-like brushite crystals along plane (020) (BCu0 with Ca:P molar ratio 1) is illustrated in Figure 4A. Characteristic of the morphology of brushite is the appearance of a plate-like or needle-like structure, depending on the pH solution used [9–11]. The plate-like crystals are thin (≈500 nm), although their width and elongation are approximately 20 μm and 40 μm, respectively. Values are similar to these are reported in other studies [9,32]. As the Cu/Ca molar ratio increases to 0.25—hence, a higher degree of Ca replacement with Cu as well as sampleite-like precipitation (BCu2) takes place—brushite crystals of smaller length are formed, ranging ≈10 μm to ≈20 μm in that direction (020) (Figure 4B), as found in an earlier study [33,34]. Figure 4C–E shows that BCu4, BCu5, and BCu6 exhibit similar crystal morphology and sizes of sampleite-like material, comprising monoclinic crystals with a length of ≈5 μm. The material BCu10, having semi-crystalline or an amorphous structure, is eventually formed. SEM analysis confirms the XRD results shown in Figure 2.

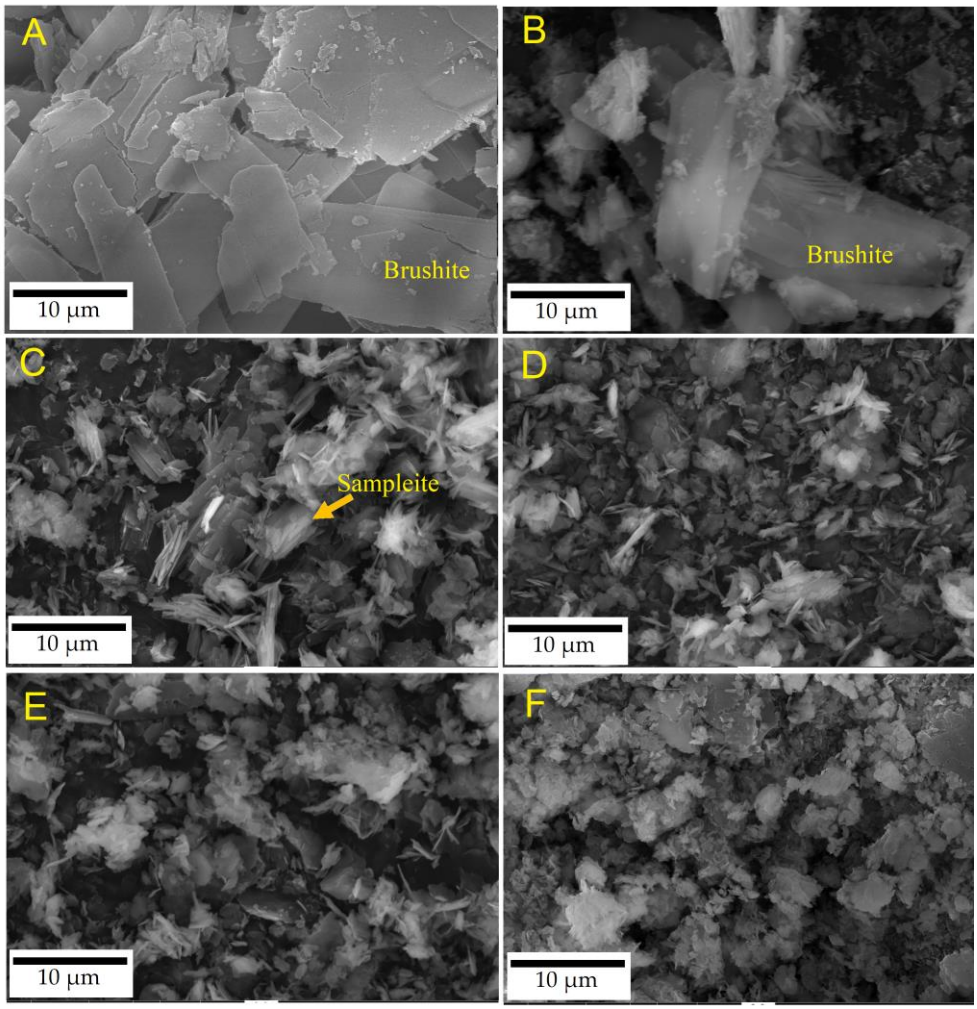

Figure 4. SEM images of Ca-Cu phosphates, (**A**) BCu0, (**B**) BCu1, (**C**) BCu4, (**D**) BCu5, (**E**) BCu6, and (**F**) BCu10 (all images have the same 10 μm scale bar).

The EDX analysis, as shown in Figure 5A–E, shows an increasing trend—from BCu0 up to BCu10—in Cu contents, with an increasing Cu/Ca molar ratio in the starting solutions. Greater Na contents are likewise observed accompanied with an increase in Cu. Peaks corresponding to Ca disappeared in the BCu10 compound; see Figure 5E.

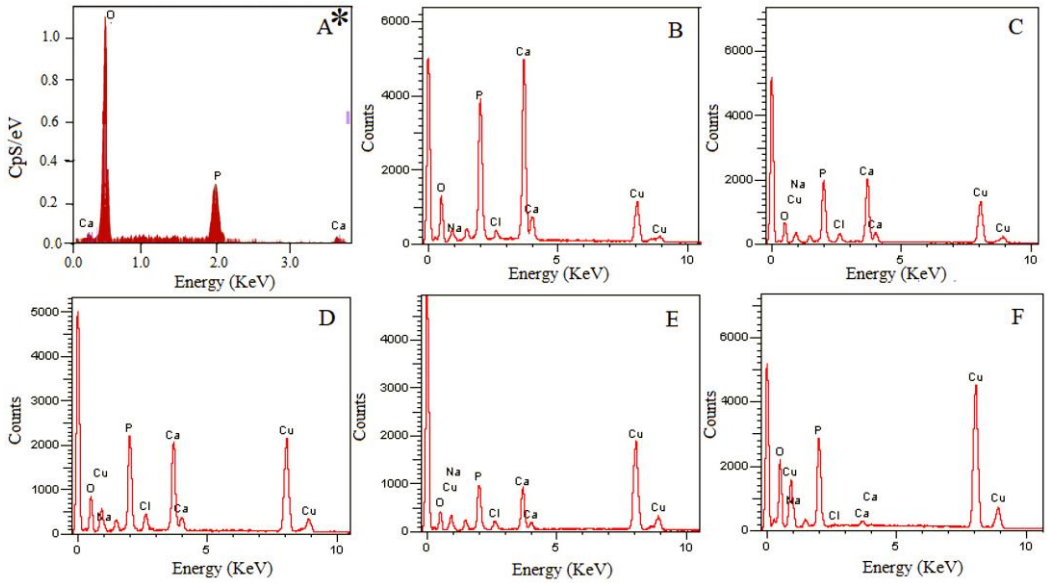

Figure 5. EDX analysis of (**A**) BCu0, (**B**) BCu2, (**C**) BCu4, (**D**) BCu5, (**E**) BCu6, and (**F**) BCu10 compounds. * Different scale of measurements.

A summary of elemental analysis is offered in Table 4. The atomic percentages (BCu0) of Ca, P, and O were respectively 17.83, 14.74, and 67.42 [31], nearly matching the theoretical composition of brushite, namely 23.25, 18.20, and 55.80 wt %, respectively. Increasing the percentages of the Cu/Ca molar ratio from 0, BCu0, up to 1.5, BCu6, results in increased Cl as well as Na wt%. These two elements, which tend to bond with Cu, Cl, and Na, are necessary to form sampleite-like mineral ($NaCaCu_5(PO_4)_4Cl{\cdot}5H_2O$). The percentages reported prove that the Cu present in the solution replaced Ca and bonded with Na and Cl to form sampleite-like mineral [34]. The role of Cu incorporation into the lattice of the produced materials is very important, since it increases their elasticity and allows for their use as bioceramics in medical applications. Still, the elucidation of sampleite-like mineral incorporation and its effect on the properties of (bio)materials need to be further investigated.

Table 4. Chemical composition of the Ca-Cu compounds in atomic% based on the EDX analysis (Figure 5).

	BCu0	BCu2	BCu4	BCu5	BCu6	BCu10
O	55.8	56.31	43.67	40.15	28.83	41.43
Na	0	1.05	2.26	2.16	2.7	5.99
P	18.20	14.06	14.67	13.68	10.93	11.58
Cl	0	0.86	1.96	2.12	1.81	0.16
Ca	23.25	17.52	13.74	11.25	8.47	0.45
Cu	0	10.2	23.71	30.64	47.25	40.38

3.2. Thermogravimetric Analysis (TGA)

The results of the TGA analysis for the Ca-Cu phosphate compounds are shown in Figure 6. Brushite is classified as a water-bearing phosphate [34,35] containing two molecules of structural water in its lattice and free water on its surface, as indicated by the presence of two sharp peaks of mass loss during heating at 80–220 °C [9]. During the transformation of brushite to monetite, $CaHPO_4$, at ≈220 °C [36], and later to calcium pyrophosphate, $Ca_2P_2O_7$, at ≈400 °C [8], part of the chemically-bound water is released. At higher temperatures of 750–800 °C [36], pyrophosphates are decomposed. The heating of pure brushite (BM0) to 600 °C results in a mass loss of approximately 25 wt %, while

the typical mass loss resulting from the dehydration and releasing of structural water of brushite is 21 wt % [37], Figure 6.

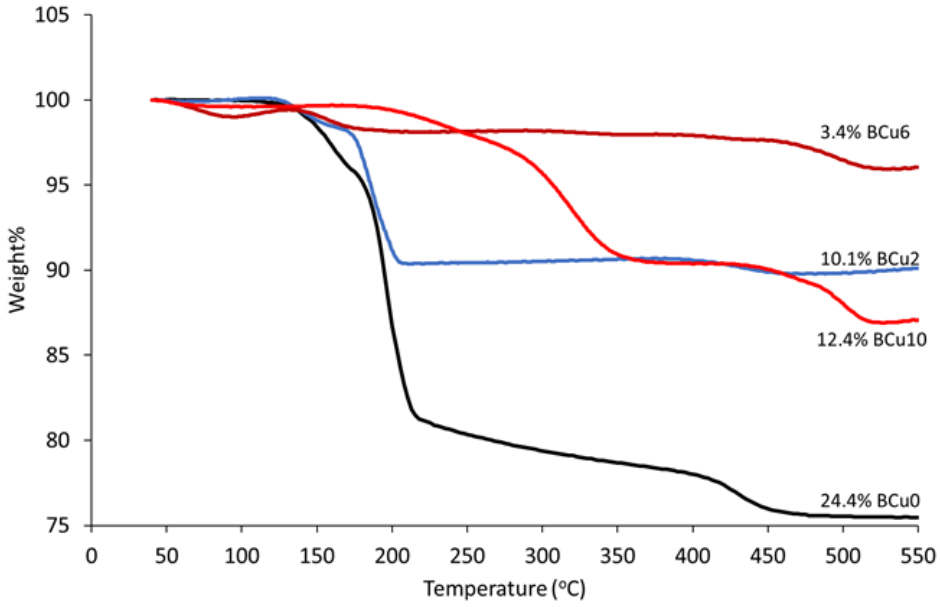

Figure 6. TG curves of Ca-Cu phosphates.

The dehydration of brushite over 215 °C takes place according to Equation (1) and normally results in a weight loss of about 19 wt %, while the formation of calcium pyrophosphate is accomplished by the following equations [38–40]:

$$CaHPO_4 \cdot 2H_2O \rightarrow CaHPO_4 + 2H_2O \quad (1)$$

$$2CaHPO_4 \rightarrow Ca_2P_2O_7 + H_2O. \quad (2)$$

The mass loss determined for biphasic phosphates (BCu2) decreases to 10.1 wt %, which is lower than for pure brushite [23]. The mass loss of sampleite, BCu4, is due to the loss of moisture or the release of structural water.

Differential thermogravimetric patterns for Ca-Cu phosphates are shown in Figure 7. Figure 7A,B show, respectively, the dehydration peaks associated with the two structural water molecules of pure brushite (BCu0) as well as those of the biphasic phosphates produced with Cu/Ca ratios 0.25 (BCu2), which are characterized by precipitation of brushite and sampleite-like minerals together. When the Cu/Ca ratio in the starting solution increases to the range of 0.67 and 1.5 (BCu4, BCu5, and BCu6, Figure 7C), three zones of mass loss at approximately 80 °C, 160 °C, and 500 °C are seen. Meanwhile, Figure 7D shows the loss of structural water of amorphous copper phosphates (BCu10) for which the overall mass loss at 550 °C was approximately 12.4%. Two mass loss peaks are shown at 320 °C and 500 °C, under sampleite-like heating (BCu10) up to 550 °C; see Figure 7D.

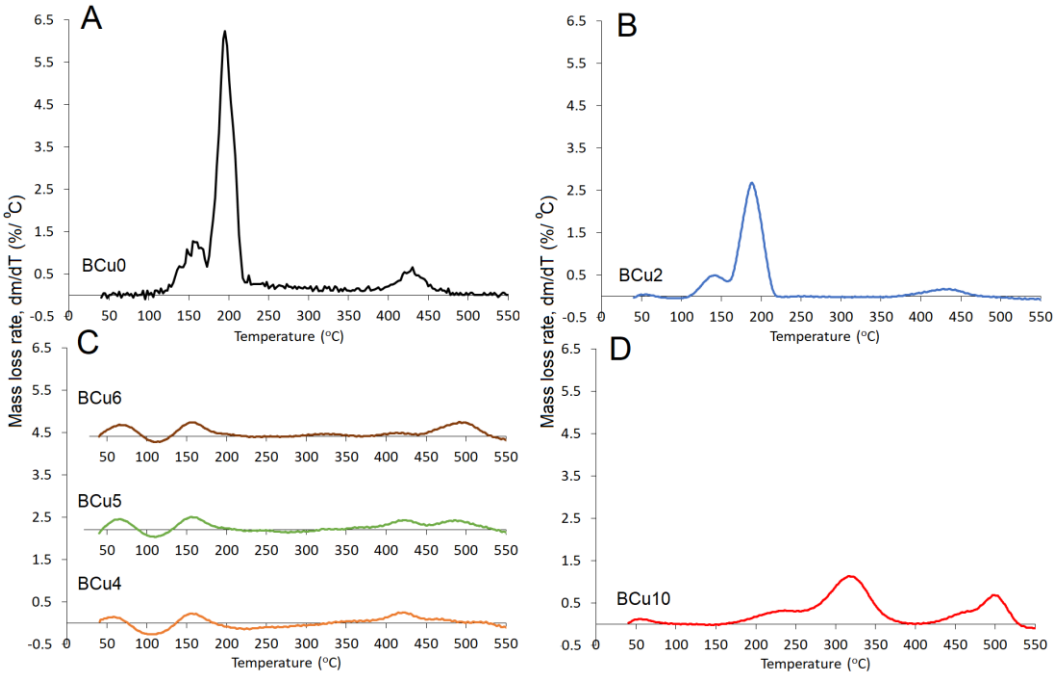

Figure 7. Differential thermogravimetric analysis (TGA) of Ca-Cu phosphates, (**A**) BCu0, (**B**) BCu2, (**C**) BCu4, BCu5, and BCu6, and (**D**) BCu10 compounds.

3.3. Phase Evolution during the Precipitation of $Ca_{1-x}Cu_xHPO_4 \cdot nH_2O$ Compounds

The results of this study demonstrated that biphasic phosphate minerals—brushite and sampleite-like minerals—form when the Cu/Ca ratio in the starting solution is up to 0.25. A monoclinic crystalline structure characterizes both minerals. The main difference noticed is the decrease in brushite crystal size owing to crystal growth inhibition induced by copper.

As the Cu/Ca ratio increases to 0.67, and eventually to 1.5 (BCu4–BCu6), only sampleite-like mineral starts to precipitate after bonding with Cl and Na. When no Ca is present in the starting solution, a semi-crystalline or amorphous structure precipitates (BCu10). These data are summarized below in Table 5.

Table 5. Phase evolution, crystal size, and structure as functions of Cu/Ca molar ratio in solution.

Cu/Ca Ratio	Crystal Structure	Crystal Size (μm)	Compounds Formed
0	monoclinic	~40	Brushite
$0 \leq 0.25$	monoclinic	~15 + ~5	Brushite + sampleite-like
$0.25 < x \leq 1.5$	monoclinic	~5	Sampleite-like
$1.5 \leq x$	-	-	Semi-crystalline

4. Conclusions

With the use of XRD, TG, and SEM analysis in this study, the evolution of the degree of replacement of Ca by Cu in brushite—for the synthesis of $Ca_{1-x}Cu_xHPO_4 \cdot nH_2O$ materials—was investigated and elucidated.

It is shown that a low Cu/Ca molar ratio (up to 0.25 in the starting solution) results in the precipitation of biphasic phosphate materials: brushite and sampleite-like minerals. Increasing the Cu/Ca molar ratio gradually to 1.5 while the solution superstation with respect to Cu increases leads to monoclinic sampleite-like precipitates.

Useful insights were gained in this research for a future synthesis of biomaterials with specific compositions and tailored properties by controlling the Cu/Ca ratio in the starting solution. Further investigations would be needed to elucidate several aspects regarding the performance of the produced biomaterials. Factors surrounding their biological and

mechanical performance, as well as physicochemical and antibacterial properties, call for careful exploration. Likewise, further studies on the effect of doping with additional ions are needed, since specific ions might exhibit either beneficial or detrimental effects on the finally desired properties of the produced biomaterials.

Sampleite is a rare mineral [34,41] discovered in 1942. This study presents a novel method for its synthesis. While brushite is considered as a precursor of biomaterial and a source of Ca ions, sampleite could prove to be a promising source of Cu ions and a precursor of biomaterials. In the near future, studies might focus on the synthesis and use of this mineral in biomedical applications.

Author Contributions: Conceptualization, K.I. and M.A.; methodology, M.A. and G.S. and K.I.; validation, M.A., G.S. and J.A.-K.; formal analysis, K.I., and M.A.; powder synthesis and characterization, A.S.A. and M.A.; investigation, M.A., A.S.A. and N.H.; resources, M.A. and A.S.A.; data curation, M.A., J.A.-K. and A.S.A.; writing—original draft preparation, M.A., G.S. and K.I.; writing—review and editing, M.A., G.S. and K.I.; supervision, K.I., M.A. and G.S. All authors have read and agreed to the published version of the manuscript.

Funding: This research received no external funding.

Institutional Review Board Statement: Not applicable.

Informed Consent Statement: Not applicable.

Data Availability Statement: The data presented in this study are available on request from the corresponding author. Most of this data is obtained after the use of analytical techniques (XRD, TG, SEM-EDS, XRS).

Conflicts of Interest: The authors declare no conflict of interest.

References

1. Alshaaer, M.; Kailani, M.H.; Ababneh, N.; Abu Mallouh, S.A.; Sweileh, B.; Awidi, A. Fabrication of porous bioceramics for bone tissue applications using luffa cylindrical fibres (LCF) as template. *Process. Appl. Ceram.* **2017**, *11*, 13–20. [CrossRef]
2. Radwan, N.H.; Nasr, M.; Ishak, R.A.; Abdeltawab, N.F.; Awad, G.A. Chitosan-calcium phosphate composite scaffolds for control of post-operative osteomyelitis: Fabrication, characterization, and in vitro–in vivo evaluation. *Carbohydr. Polym.* **2020**, *244*, 116482. [CrossRef]
3. Li, H.; Yao, Q.-Z.; Wang, Y.-Y.; Li, Y.-L.; Zhou, G.-T. Biomimetic synthesis of struvite with biogenic morphology and implication for pathological biomineralization. *Sci. Rep.* **2015**, *5*, 7718. [CrossRef] [PubMed]
4. Wu, F.; Wei, J.; Guo, H.; Chen, F.; Hong, H.; Liu, C. Self-setting bioactive calcium–magnesium phosphate cement with high strength and degradability for bone regeneration. *Acta Biomater.* **2008**, *4*, 1873–1884. [CrossRef] [PubMed]
5. Khalifehzadeh, R.; Arami, H. Biodegradable calcium phosphate nanoparticles for cancer therapy. *Adv. Colloid Interface Sci.* **2020**, *279*, 102157. [CrossRef] [PubMed]
6. Shyong, Y.-J.; Chang, K.-C.; Lin, F.-H. Calcium phosphate particles stimulate exosome secretion from phagocytes for the enhancement of drug delivery. *Colloids Surf. B Biointerfaces* **2018**, *171*, 391–397. [CrossRef] [PubMed]
7. Liu, Y.; Ma, R.; Li, D.; Qi, C.; Han, L.; Chen, M.; Fu, F.; Yuan, J.; Li, G. Effects of calcium magnesium phosphate fertilizer, biochar and spent mushroom substrate on compost maturity and gaseous emissions during pig manure composting. *J. Environ. Manag.* **2020**, *267*, 110649. [CrossRef] [PubMed]
8. Alshaaer, M.; Cuypers, H.; Mosselmans, G.; Rahier, H.; Wastiels, J. Evaluation of a low temperature hardening Inorganic Phosphate Cement for high-temperature applications. *Cem. Concr. Res.* **2011**, *41*, 38–45. [CrossRef]
9. Alshaaer, M. Microstructural characteristics and long-term stability of wollastonite-based chemically bonded phosphate ceramics. *Int. J. Appl. Ceram. Technol.* **2021**, *18*, 319–331. [CrossRef]
10. Alkhraisat, M.H.; Rueda, C.; Cabarcos, E.L. Strontium Ions Substitution in Brushite Crystals: The Role of Strontium Chloride. *J. Funct. Biomater.* **2011**, *2*, 31–38. [CrossRef]
11. Xue, Z.; Wang, Z.; Sun, A.; Huang, J.; Wu, W.; Chen, M.; Hao, X.; Huang, Z.; Lin, X.; Weng, S. Rapid construction of poly-etheretherketone (PEEK) biological implants incorporated with brushite (CaHPO4·2H2O) and antibiotics for anti-infection and enhanced osseointegration. *Mater. Sci. Eng. C Mater.* **2020**, *111*, 110782. [CrossRef] [PubMed]
12. Kim, Y.; Lee, S.Y.; Roh, Y.; Lee, J.; Kim, J.; Lee, Y.; Bang, J.; Lee, Y.J. Optimizing Calcium Phosphates by the Control of pH and Temperature via Wet Precipitation. *J. Nanosci. Nanotechnol.* **2015**, *15*, 10008–10016. [CrossRef] [PubMed]
13. Luo, J.; Engqvist, H.; Persson, C. A ready-to-use acidic, brushite-forming calcium phosphate cement. *Acta Biomater.* **2018**, *81*, 304–314. [CrossRef]
14. Huotari, K.; Peltola, M.; Jämsen, E. The incidence of late prosthetic joint infections. *Acta Orthop.* **2015**, *86*, 321–325. [CrossRef]

15. Vincent, M.; Duval, R.; Hartemann, P.; Engels-Deutsch, M. Contact killing and antimicrobial properties of copper. *J. Appl. Microbiol.* **2018**, *124*, 1032–1046. [CrossRef]
16. Colin, M.; Carré, G.; Klingelschmitt, F.; Reffuveille, F.; Gangloff, S. Copper alloys to prevent bacterial biofilm formation on touch surfaces. *Mater. Lett.* **2021**, *305*, 130712. [CrossRef]
17. Blades, B.; Ayton, S.; Hung, Y.H.; Bush, A.I.; La Fontaine, S. Copper and lipid metabolism: A reciprocal relationship. *Biochim. Et Biophys. Acta (BBA) Gen. Subj.* **2021**, *1865*, 129979. [CrossRef]
18. Mert, I.; Mandel, S.; Tas, A.C. Do cell culture solutions transform brushite (CaHP04.2H20) to octacalium phosphate (Ca8(HP04)2(P04)4 5H20). In *Advances in Bioceramics and Porous Ceramics IV*; Narayan, R., Colombo, P., Eds.; John Wiley & Sons Inc.: Hoboken, NJ, USA, 2011; pp. 79–94. [CrossRef]
19. Kargozar, S.; Mozafari, M.; Ghodrat, S.; Fiume, E.; Baino, F. Copper-containing bioactive glasses and glass-ceramics: From tissue regeneration to cancer therapeutic strategies. *Mater. Sci. Eng. C* **2021**, *121*, 111741. [CrossRef]
20. Kargozar, S.; Baino, F.; Hamzehlou, S.; Hill, R.G.; Mozafari, M. Bioactive Glasses: Sprouting Angiogenesis in Tissue Engineering. *Trends Biotechnol.* **2018**, *36*, 430–444. [CrossRef]
21. Hongfeng, Z.; El-Kott, A.; Ahmed, A.E.; Khames, A. Synthesis of chitosan-stabilized copper nanoparticles (CS-Cu NPs): Its catalytic activity for C-N and C-O cross-coupling reactions and treatment of bladder cancer. *Arab. J. Chem.* **2021**, *14*, 103259. [CrossRef]
22. Jin, S.; Ren, L.; Yang, K. Bio-Functional Cu Containing Biomaterials: A New Way to Enhance Bio-Adaption of Biomaterials. *J. Mater. Sci. Technol.* **2016**, *32*, 835–839. [CrossRef]
23. Pina, S.; Olhero, S.; Gheduzzi, S.; Miles, A.; Ferreira, J. Influence of setting liquid composition and liquid-to-powder ratio on properties of a Mg-substituted calcium phosphate cement. *Acta Biomater.* **2009**, *5*, 1233–1240. [CrossRef]
24. Schorn, S.; Hock, E.; Linde, C.; Blümner, P.; Gäbelein, M.; Schluchti, T.; Annacker, V.; Brand, A.; de Wit, F.; Diether, D.; et al. "Mineral Atlas—Fossil Atlas". Available online: https://www.mineralienatlas.de/lexikon/index.php/MineralData?mineral=Sampleite (accessed on 21 August 2021).
25. Hurle, K.; Oliveira, J.; Reis, R.; Pina, S.; Goetz-Neunhoeffer, F. Ion-doped Brushite Cements for Bone Regeneration. *Acta Biomater.* **2021**, *123*, 51–71. [CrossRef]
26. Sayahi, M.; Santos, J.; El-Feki, H.; Charvillat, C.; Bosc, F.; Karacan, I.; Milthorpe, B.; Drouet, C. Brushite (Ca,M)HPO4, 2H2O doping with bioactive ions (M = Mg2+, Sr2+, Zn2+, Cu2+, and Ag+): A new path to functional biomaterials? *Mater. Today Chem.* **2020**, *16*, 100230. [CrossRef]
27. Alshaaer, M.; Abdel-Fattah, E.; Saadeddin, I.; Al Battah, F.; Issa, K.I.; Saffarini, G. The effect of natural fibres template on the chemical and structural properties of Biphasic Calcium Phosphate scaffold. *Mater. Res. Express* **2020**, *7*, 065405. [CrossRef]
28. Alshaaer, M.; Afify, A.S.; Moustapha, M.E.; Hamad, N.; Hammouda, G.A.; Rocha, F. Effects of the full-scale substitution of strontium for calcium on the microstructure of brushite: $(CaxSr_{1-x})HPO_4.nH_2O$ system. *Clay Miner.* **2020**, *55*, 366–374. [CrossRef]
29. Patil, S.B.; Jena, A.; Bhargava, P. Influence of Ethanol Amount During Washing on Deagglomeration of Co-Precipitated Calcined Nanocrystalline 3YSZ Powders. *Int. J. Appl. Ceram. Technol.* **2012**, *10*, E247–E257. [CrossRef]
30. Piva, R.H.; Piva, D.H.; Pierri, J.; Montedo, O.R.K.; Morelli, M.R. Azeotropic distillation, ethanol washing, and freeze drying on coprecipitated gels for production of high surface area 3Y–TZP and 8YSZ powders: A comparative study. *Ceram. Int.* **2015**, *41*, 14148–14156. [CrossRef]
31. Lu, B.-Q.; Willhammar, T.; Sun, B.-B.; Hedin, N.; Gale, J.D.; Gebauer, D. Introducing the crystalline phase of dicalcium phosphate monohydrate. *Nat. Commun.* **2020**, *11*, 1546. [CrossRef] [PubMed]
32. Nosrati, H.; Le, D.Q.S.; Emameh, R.Z.; Perez, M.C.; Bünger, C.E. Nucleation and growth of brushite crystals on the graphene sheets applicable in bone cement. *Bol. Soc. Esp. Cerám. Vidr.* **2020**. (In Press) [CrossRef]
33. Zhao, J.; Dong, J.; Ye, X.; Wang, L. A promising novel red-emitting Eu3+-activated neodymium calcium phosphate phosphor with good thermal stability and excellent color purity for WLEDs. *J. Mol. Struct.* **2021**, *1240*, 130567. [CrossRef]
34. Lagier, R.; Baud, C.-A. Magnesium Whitlockite, a Calcium Phosphate Crystal of Special Interest in Pathology. *Pathol. Res. Pr.* **2003**, *199*, 329–335. [CrossRef]
35. Girişken, G.; Tas, A. Development of biomineralization solutions to facilitate the transformation of brushite (Ca-HPO4·2H2O) into octacalcium phosphate (Ca8(HPO4)2(PO4)4·5H2O). In Proceedings of the 15th National Biomedical Engineering Meeting (BIYOMUT), Antalya, Turkey, 21–24 April 2010; pp. 1–4. [CrossRef]
36. Alshaaer, M.; Issa, K.; Alanazi, A.; Mallouh, S.; Afify, A.; Moustapha, M.; Komnitsas, K. Gradual Replacement of Ca^{2+} with Mg^{2+} Ions in Brushite for the Production of $Ca_{1-x}Mg_xHPO_4{\cdot}nH_2O$ Materials. *Minerals* **2021**, *11*, 284. [CrossRef]
37. Alshaaer, M.; Cuypers, H.; Rahier, H.; Wastiels, J. Production of monetite-based Inorganic Phosphate Cement (M-IPC) using hydrothermal post curing (HTPC). *Cem. Concr. Res.* **2011**, *41*, 30–37. [CrossRef]
38. Dosen, A.; Giese, R.F. Thermal decomposition of brushite, CaHPO4{middle dot}2H2O to monetite CaHPO4 and the formation of an amorphous phase. *Am. Miner.* **2011**, *96*, 368–373. [CrossRef]
39. Tortet, L.; Gavarri, J.R.; Nihoul, G.; Dianoux, A. Study of Protonic Mobility in CaHPO4·2H2O (Brushite) and $CaHPO_4$ (Monetite) by Infrared Spectroscopy and Neutron Scattering. *J. Solid State Chem.* **1997**, *132*, 6–16. [CrossRef]
40. Frost, R.L.; Palmer, S.J. Thermal stability of the 'cave' mineral brushite CaHPO4·2H2O—Mechanism of formation and decomposition. *Thermochim. Acta* **2011**, *521*, 14–17. [CrossRef]
41. Mindat.org. Available online: https://www.mindat.org/min-3515.html (accessed on 9 September 2021).